Research Article | Vol. 25, No. 23 | 13 Nov 2017 | OPTICS EXPRESS 28478
Optics EXPRESS

In-situ microscopy of front and rear side ablation processes in alkali aluminosilicate glass using ultra short pulsed laser radiation

DANIEL GROSSMANN,[1,2,*] MARTIN REININGHAUS,[3,2] CHRISTIAN KALUPKA,[2] MICHAEL JENNE,[1] AND MALTE KUMKAR[1]

[1] *TRUMPF Laser- und Systemtechnik GmbH, Johann-Maus-Strasse 2, 71254 Ditzingen, Germany*
[2] *Chair for Laser Technology, RWTH Aachen University, Steinbachstr 15, 52074 Aachen, Germany*
[3] *Fraunhofer Institute for Laser Technology ILT, Steinbachstr 15, 52074 Aachen, Germany*
[*] *daniel.grossmann@de.trumpf.com*

Abstract: The visualization of the nonlinear absorption, the subsequent relaxation of excited states and the formation of defects enables the investigation of fundamental laser-material-interaction as well as the identification of process windows for micromachining of transparent materials with ultra short pulsed laser radiation. In this work, time resolved pump probe microscopy is applied to analyze the laser-material-interaction and to reduce damage inside the material during front- and rear side ablation of nonstrengthened Corning Gorilla glass. The experiments give an insight into the pulse duration dependence of the absorption zone, the influence of the surface geometry, in-volume damage and the formation of transient visible cracks.

OCIS codes: (100.0118) Imaging ultrafast phenomena; (320.7110) Ultrafast nonlinear optics; (320.7100) Ultrafast measurements; (140.3390) Laser materials processing.

References and links

1. S. Nisar, L. Li and M. A. Sheikh, "Laser glass cutting techniques - a review," J. Laser Appl. **25**, 042010 (2013).
2. M. Malinauskas, A. Zukauskas, S. Hasegawa, Y. Hayasaki, V. Mizeikis, R. Buividas and S. Juodkazis, "Ultrafast laser processing of materials: from science to industry," Light Sci. Appl. **5**, e16133 (2016).
3. Y. Li, K. Itoh, W. Watanabe, K. Yamada, D. Kuroda, J. Nishii and Y. Jiang, "Three-dimensional hole drilling of silica glass from the rear surface with femtosecond laser pulses," Opt. Lett. **26**, 1912–1914 (2001).
4. A. Marcinkevicius, S. Juodkazis, M. Watanabe, M. Miwa, S. Matsuo, H. Misawa and J. Nishii, "Femtosecond laser-assisted three-dimensional microfabrication in silica," Opt. Lett. **26**, 277–279 (2001).
5. M. Ehrhardt, G. Raciukaitis, P. Gecys and K. Zimmer, "Laser-induced backside wet etching of fluoride and sapphire using picosecond laser pulses," Appl. Phys. A **101**, 399–404 (2010).
6. B. C. Stuart, M. D. Feit, A. M. Rubenchik, B. W. Shore and M. D. Perry, "Laser-induced damage in dielectrics with nanosecond to subpicosecond pulses," Phys. Rev. Lett. **74**, 2248 (1995).
7. M. Garcia-Lechuga, J. Solis and Jan Siegel, "Melt front propagation in dielectrics upon femtosecond laser irradiation: formation dynamics of a heat-affected layer," Appl. Phys. Lett. **108**, 171901 (2016).
8. E. G. Gamaly, A. V. Rode, B. Luther-Davies and V. T. Tikhonchuk, "Ablation of solids by femtosecond lasers: ablation mechanism and ablation thresholds for metals and dielectrics," Phys. Plasmas. **9**, 949 (2002).
9. L. Shah, J. Tawney, M. Richardson and K. Richardson, "Femtosecond laser deep hole drilling of silicate glasses in air," Appl. Surf. Science **183**, 151–164 (2001).
10. M. Sun, U. Eppelt, C. Hartmann, W. Schulz, J. Zhu and Z. Lin, "Damage morphology and mechanism in ablation cutting of thin glass sheets with picosecond pulsed lasers," Opt. Laser Technol. **80**, 227–236 (2016).
11. S. S. Mao, F. Quere, S. Guizard, X. Mao, R.E. Russo, G. Petite and P. Martin, "Dynamics of femtosecond laser interactions with dielectrics," Appl. Phys. A **79**, 1695–1709 (2004).
12. Q. Sun, H. Jiang, Y. Liu, Z. Wu, H. Yang, and Q. Gong, "Measurement of the collision time of dense electronic plasma induced by a femtosecond laser in fused silica," Opt. Lett. **30**, 320–322 (2005).
13. D. Puerto, W. Gawelda, J. Siegel, J. Bonse, G. Bachelier and J. Solis, "Transient reflectivity and transmission changes during plasma formation and ablation in fused silica induced by femtosecond laser pulses," Appl. Phys. A **92**, 803–808 (2008).
14. S. Rapp, M. Kaiser, M. Schmidt and H. P. Huber, "Ultrafast pump-probe ellipsometry setup for the measurement of transient optical properties during laser ablation," Opt. Express. **24**, 17572–17592 (2016).
15. J. Koch, S. Heiroth, T. Lippert and D. Guenther, "Femtosecond laser ablation: visualization of the aerosol formation process by light scattering and shadowgraphic imaging," Spectrochim. Acta B At. Spectrosc. **65**, 943–949 (2010).

#304446 https://doi.org/10.1364/OE.25.028478
Journal © 2017 Received 14 Aug 2017; revised 15 Oct 2017; accepted 16 Oct 2017; published 2 Nov 2017

Optics EXPRESS

16. S. G. Demos, R. A. Negres, R. N. Raman, M. D. Feit, K. R. Manes and A. M. Rubenchik, "Relaxation dynamics of nanosecond laser superheated material in dielectrics ," Optica **2**, 765–772 (2015).
17. D. Grossmann, M. Reininghaus, C. Kalupka, M. Kumkar and R. Poprawe, "Transverse pump-probe microscopy of moving breakdown, filamentation and self-organized absorption in alkali aluminosilicate glass using ultrashort pulse laser ," Opt. Express **24**, 23221–23231 (2016).
18. C. Kalupka, D. Grossmann and M. Reininghaus, "Evolution of energy deposition during glass cutting with pulsed femtosecond laser radiation ," Appl. Phys. A **123**, 376 (2017).
19. K. Bergner, B. Seyfarth, M. Kumkar, A. Tünnermann and S. Nolte, "Time-resolved microscopy for optimizing in-volume glass processing using ultra short laser pulses ," in Conference on Lasers and Electro-Optics, OSA Technical Digest (online) (Optical Society of America, 2016), paper ATu4K.1.
20. M. Kumkar, L. Bauer, S. Russ, M. Wendel, J. Kleiner, D. Grossmann, K. Bergner and S. Nolte, "Comparison of different processes for separation of glass and crystals using ultrashort pulsed lasers," Proc. SPIE **8972**, 897214 (2014).
21. W. Kautek, J. Krüger, M. Lenzner, S. Sartania, C. Spielmann and F. Krausz, "Laser ablation of dielectrics with pulse durations between 20 fs and 3 ps ," Appl. Phys. Lett. **69**, 3146 (1996).
22. E. G. Gamaly, S. Juodkazis, K. Nishimura, H. Misawa, B. Luther-Davies, L. Hallo, P. Nicolai, and V. T. Tikhonchuk, "Laser-matter interaction in the bulk of a transparent solid: confined microexplosion and void formation," Phys. Rev. B **73**, 214101 (2006).
23. M. Sakakura, T. Tochio, M. Eida, Y. Shimotsuma, S. Kanehira, M. Nishi, K. Miura, and K. Hirao, "Observation of laser-induced stress waves and mechanism of structural changes inside rock-salt crystals," Opt. Express **19**, 17780–17789 (2011).
24. F. Berto, P. Lazzarin, "Recent developments in brittle and quasi-brittle failure assessment of engineering materials by means of local approaches," Materials Science and Engineering **75**, 1–48 (2014).
25. F. Hendricks, V. V. Matylisky, M. Domke, and H. P. Huber, "Time-resolved study of femtosecond laser induced micro-modifications inside transparent brittle materials," Proc. SPIE **9740**, 97401A (2016).
26. M. Hermans, J. Gottmann, and F. Riedel, "Selective, laser-induced etching of fused silica at high scan-speeds using KOH," J. Laser Micro Nanoeng. **9**, 126–131 (2014).

1. Introduction

Ultra short pulsed laser ablation of transparent materials is an industrial established technology that meets the demands for versatile structuring of wide band gap materials with minimal damage, especially for consumer electronics and semiconductor industry [1, 2].

These advantages are attributed to the unique interaction between the ultra short pulsed laser radiation and the material. For the following work, we want to emphasize two underlying effects.

First, the dominant initial absorption process is nonlinear. Therefore, the pulse energy can be deposited in strongly confined local regions. This characteristic effect is used for processes like rear side ablation [3], volume modification with subsequent etching [4] or laser induced back side wet etching [5].

Second, the electron-phonon-coupling on a femtosecond to picosecond timescale is longer or in the order of the pulse duration. During the nonlinear absorption, the pulse energy primarily heats the electron subsystem via multiphoton, tunnel and avalanche ionization and thermalization occurs subsequent to the absorption process [6, 7].

When the lattice is heated, various ablation processes can follow at the glass-air interface in dependence of the process parameters. Mechanisms like vaporization, phase explosion or non-thermal melting have been discussed in this context [8, 9].

Basically, in all of these processes material is ablated or expelled from the target and just a part of the deposited energy remains in the sample. This residual energy can lead to various defects, cracks, material modifications or a heating of the workpiece. For a maximized breaking strength of the processed glasses and crystals, this damaged regions as well as the heat affected zones (HAZ) should be minimized [10].

To generate a more detailed understanding of the underlying mechanisms and to identify parameters for an optimized process regime, in-situ investigations by pump-probe microscopy provide access to the complex interplay of the afore mentioned effects.

Pump-probe investigations were carried out to analyze the generation of in-volume modifications [11, 12]. For ablation processes, this technique has been applied in reflectance and transmission

Optics EXPRESS

to investigate the temporal evolution of absorption and ablation processes [13], the formation dynamics of the HAZ [7] or the complex refractive index by time resolved ellipsometry [14]. Other studies provide insight into the pressure wave formation and ablation products at the workpiece surface for femtosecond [15] and nanosecond laser processing [16].

Additional experimental data of damage mechanisms inside the material on different timescales and various ablation regimes will help to develop a more detailed understanding to optimize ablation processes. Hence, we conducted experiments to address the investigation of material defects for two different ablation processes to pursue prior work [17, 18].

We will start with a short overview of our experimental setup and analyze several damage mechanisms of two different ablation processes subsequently.

First, we begin with a classical front side ablation process. Our observations show the absorption zone in the glass under the influence of a crater formation. We compare pulse durations of 100 fs and 5 ps to consider their impact on rear side damage. Additionally, we analyze the damage mechanisms on different timescales and report the formation of transient visible cracks.

Second, our investigations are carried out for a rear side ablation process. We analyze the absorption zone for different focal positions and observe the influence of incubation effects. Finally, we examine optimized parameters which enable material ablation with minimal damage and reduced taper angles.

2. Experimental setup

For our in-situ ablation experiments we used a pump-probe microscope. A detailed description of our setup and imaging methods can be found elsewhere [17]. In the following part we will summarize the essential specifications.

Our setup comprises a titanium-sapphire laser which operates at a wavelength of 800 nm and at a pulse duration of 100 fs with a maximum pulse energy of 2 mJ. To process materials at different pulse durations, our setup contains an an external double pass grating stretcher in the pump beamline. The following experiments were carried out with a pump pulse duration of 100 fs and 5 ps, as well as a spatial Gaussian beam profile and linear polarization. The raw beam diameter is 6 mm. Our in-situ imaging system uses a linear polarized, frequency doubled radiation at a wavelength of 400 nm and a constant pulse duration of 100 fs, which is independent from the parameters of the pump beam. The temporal resolution is approximately 100 fs and the spatial resolution is sub 10 µm. Our imaging system comprises a band-pass filter at 400 nm to reduce plasma luminescence and block scattered pump radiation.

The samples consist of alkali-aluminium-silica glass (nonstrengthened Corning Gorilla glass) with a thickness of 700 µm. We conducted all experiments in this work on nonstrengthened glass to avoid additional effects, caused by the ion exchanged regions, which result from a chemical strengthening process. Our samples where polished on one edge to allow in-situ microscopy of volume effects. All experiments were carried out in a standard room environment after cleaning the samples with high purity methanol.

All images are recorded from single shot experiments. We generate shadowgraph images I_s and background images I_0 to calculate the optical depth $\tau = \ln(I_0/I_s)$, similar to our work in [17]. The resulting images visualize the regions of nonlinear absorption with their local, integrated extinction coefficients. Therefore, the optical depth comprises effects for a reduced probe signal due to electrons and defects as well as scattering, diffraction and refraction. We describe this area, which shows an increased optical depth, as absorption zone. All delay values are relative to the first occurrence of a signal change from the background and the absorption start of the laser pulse, respectively. For multi pulse experiments with n pulses, this delay corresponds to the absorption of the n-th pulse.

Optics EXPRESS

3. Front side ablation

To investigate the absorption zone and the influence of the crater formation in an ablation process, we used a 100 fs pump pulse duration and a pulse energy of 50 µJ (calculated fluence of 22 J/cm^2) at a repetition rate of 1 Hz. The pulse was focused by a lens with a focal length of 100 mm (Rayleigh length of 283 µm) and the focal position was set to the surface. The spot size is calculated to a diameter of 17 µm. We applied a delay of 10 ps after the first change with respect to the background image became visible. At this delay the maximum extended absorption zone is detected. Moreover, the absorption zone remains almost constant for several picoseconds [17]. The corresponding images of the optical depth are presented in Fig. 1.

During the first pulse, the absorption zone has an extent of approximately 50 µm in propagation direction and then transitions to a filamentary characteristic due to an equilibrium of Kerr lens self-focusing and plasma defocussing [17]. With an increasing number of deposited pulses the crater geometry is formed. This affects the propagation in the material based on refraction and diffraction at the surface shape. The crater curvature leads to a focusing effect in the corners as a result of the convex geometry. In addition, diffraction and interference can result in a locally increased intensity [10, 18]. Originating from these points, absorption spikes are generated which spread to the side with an increasing number of pulses, until the crater on the entrance converges to a constant shape.

Furthermore, the concave crater ground shields the central filament with each additional pulse. Up to the deposition of 27 pulses a central filament can be observed.

The negative value of the optical depth in the crater is generated due to plasma luminescence at a wavelength of 400 nm.

When the crater edge geometry is finally developed after 77 pulses, the increased optical depth matches typical ablation damage structures. With the applied delay of 10 ps the recorded signal predominately visualizes the effect of an increased free-electron density. These damaged regions were reported in other publications by ex-situ microscopy and numerical simulations [10].

In-situ microscopy allows to analyze the exact distribution of the free-electron density from the experiment [19] and provides a substantial support for numerical simulations as shown in [18] at a different processing regime.

Compared to classical microscopy the damaged regions are visualized with a much higher sensitivity. Particularly, due to the fact, that the type and visibility of a permanent modification can be weak compared to the electronic excitation and the subsequent transient effects [17]. We did not observe a distinct permanent modification near the crater entrance walls by ex-situ microscopy in our experiments. However it is unambiguous that energy is deposited in these regions.

To compare the influence of the pulse duration, Fig. 2(a) shows the absorption characteristic of an ablation process with a pulse duration of 5 ps and Fig. 2(b) contains the corresponding images with a pulse duration of 100 fs. All additional parameters are unchanged compared to the experiment before. To observe rear side damage, each image shows the front and the rear side of the glass sample with a thickness of 700 µm.

The first pulse in Fig. 2(a) propagates through the sample and induces an absorption peak on the front and on the rear side. With the formation of a crater, the extent of the absorption zone changes and the aforementioned propagation effects become prominent. However, even after five pulses the increased absorption around the crater on the rear side of the sample is visible with a diameter of 10 µm. Within seven pulses, the radiation at the central rear side becomes shielded and the crater does not show any change with further pulses.

In comparison, Fig. 2(b) visualizes a filamentary absorption characteristic through the total glass thickness, but without any visible increased absorption zone on the rear side. Hence, the formation of a central rear side crater can not be observed under these conditions. This pulse dependence of the rear side damage was also reported in literature for classical ablation

Optics EXPRESS

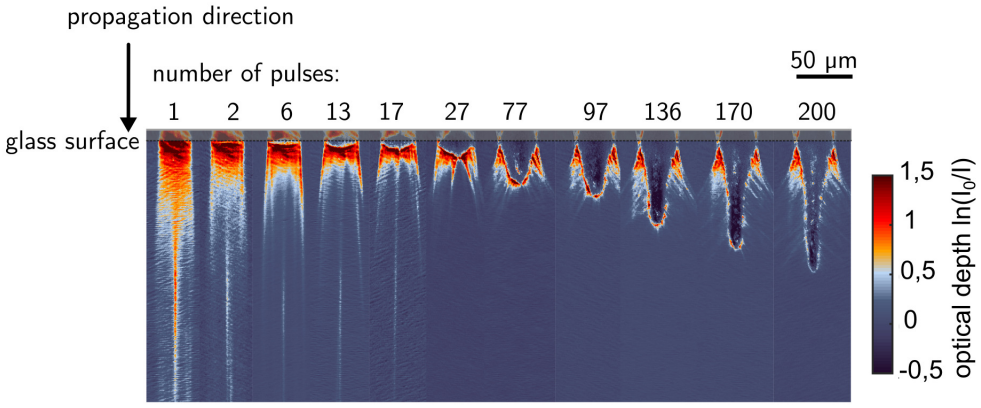

Fig. 1. Nonlinear absorption zones for different pulses during an ablation process. The pulse duration was chosen to 100 fs. The beam was focused by a lens with a focal length of 100 mm at a repetition rate of 1 Hz and a focal position on the surface. The pulse energy was set to 50 µJ. The images show the maximum absorption zone at a delay of approximately 10 ps.

experiments [20]. Additionally, in-situ microscopy shows, that the 100 fs pulse duration induces an increased free-electron density in the material up to the rear side, but without being sufficient for ablation.

When comparing the two pulse durations in Fig. 2, an additional effect can be observed. The absorption zone for the 100 fs pulse duration is much more extended into the volume below the crater, than for the pulse duration of 5 ps. However, the crater in Fig. 2(a) is more pronounced after 30 pulses compared to Fig. 2(b).

We suggest, that the much higher intensity ($4.4 \cdot 10^{14}$ W/cm^2 vs. $8.8 \cdot 10^{12}$ W/cm^2) in Fig 2(b) leads to the extended absorption zone. This might also be the reason for the difference in rear side damage. The propagation through the sample with high intensities causes absorption in the bulk, and therefore the effective pulse energy on the rear side is not sufficient for ablation.

When the ablation depth are compared, a difference between both pulse durations can be observed. This effect was already mentioned in literature [21]. The pulse duration of 100 fs generates electrons dominantly through multiphoton and tunnel ionization but not via avalanche ionization [21]. This could prevent a high localized deposited energy density in the sample compared to an avalanche dominated absorption process as shown in Fig 2(a).

To compare the electronic damage with the mechanical effects Visualization 1 shows a movie of unprocessed shadowgraph images on three timescales. Each frame in the movie represents one additional pulse. In Fig 3(a) a few selected frames are shown. The experimental conditions are the same as in the aforementioned section with a 100 fs pump pulse duration. Due to the high intensity these parameters visualize the propagation effects most clearly. However the qualitative results on a nanosecond timescale, are the same for the pulse duration of 5 ps.

The movie shows three different delays of 10 ps, 4 ns and 1 s with respect to the absorption start of the respective pulse. The textured background originates from our sample preparation process and has no further importance.

At a delay of 1 s the reduced probe signal results mostly from the ablated crater geometry due to scattering and absorption at the crater wall. In comparison, the images with a delay of 10 ps superimpose the absorption zone of the generated free-electron density as already discussed in our prior experiments. The central images at a delay of 4 ns reveal additional effects which we will discuss in the following section.

First, a spherical pressure wave in the volume below the crater can be observed. In Fig. 3(a)

Optics EXPRESS

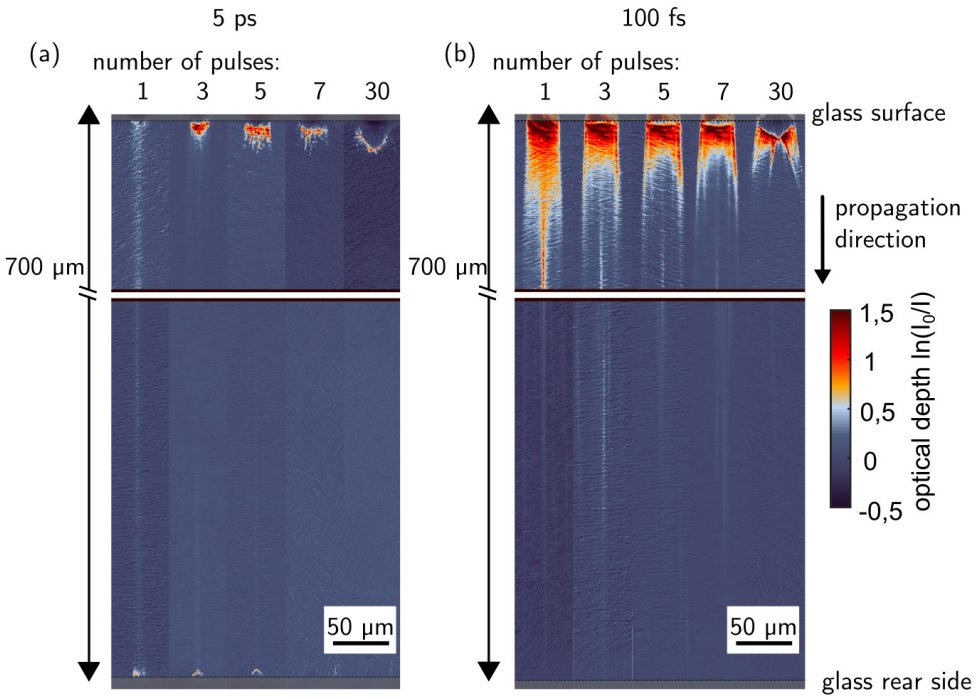

Fig. 2. Comparison of the absorption zones on the sample front and rear side. The repetition rate was set to 1 Hz. Both image parts show experiments with a pulse energy of 50 µJ focused by a lens with 100 mm focal length. The delay was chosen to approximately 10 ps, for visualizing the maximum extent of the absorption zone. In part (a) the pulse duration was set to 5 ps and in part (b) a pulse duration of 100 fs was applied.

this slightly brighter region is marked with a dashed line. This transient changed refractive index due to a compression pressure wave can most clearly be observed in the movie (Visualization 1).

Finally, a strongly reduced probe transmission, which originates from the crater ground, is visible inside the pressure wave, several nanoseconds after the pulse is absorbed. These features show a pronounced orientation perpendicular to the ablation crater. Additionally, they are not observed at a shorter delay of 10 ps or at a larger delay of 1 s. However, these regions extend beyond the initial absorption zone which is visible at a delay of 10 ps.

An additional characteristic is revealed by analyzing the deposition of subsequent pulses as shown in the movie (Visualization 1). It becomes apparent that, these features can reappear and expand along their orientation into the volume on the nanosecond timescale after this additional pulse is absorbed. The first visible appearance of these features occurs after approximately 20 pulses.

We assume, that these regions result from cracks which reduce the probe transmission due to scattering. We propose the following interpretation.

Initially, a pressure wave is generated on a nanosecond timescale due to the energy deposition in the material. This is well known from in-volume investigations [22, 23]. After a few pulses, the crater starts to form. This new surface geometry leads to a concentration of stress near the crater ground in the material, which is generally denoted as notch effect [24]. Subsequently the compressive stress from the pressure wave can open micro cracks on the crater ground. These gaps open up and expand a few micrometer into the material, when the induced stress within the pressure front is sufficiently high.

Optics EXPRESS

Within the next nanoseconds, the surface of the pressure front increases by propagation into the material and therefore the local compressive stress decreases. This stops the crack expansion and the pressure front overtakes the crack front. If the elastic limit of the surrounding material is not exceeded, the gap can close with optical contact afterwards. Therefore, these cracks are not visible at a delay of 1 s. However, the damage in the material remains and affects the breaking strength of the sample negatively. With each additional pulse this procedure is repeated. Iteratively, prior cracks can open up again and expand a few micrometer further into the material by the same mechanism.

Recently, the formation of cracks inside a pressure front was reported for volume modifications with reflective pump-probe microscopy [25]. In contrast to our experiments, these cracks where permanently visible after the process.

To test our theory and investigate the permanent material damage, we used a potassium hydroxide (KOH) solution to etch the damaged regions [26]. Figure 3(b) shows the corresponding transmission microscope images of this sample. On the left an ablated crater after 200 pulses is shown. In the right image, the identical crater after 10 minutes of etching in an 8 mol/l aqueous solution at 85 °C is presented.

The etching reveals, that the transient visible regions from Visualization 1 on a nanosecond timescale have an increased etching rate compared to the pristine glass. This characteristic is typical for material which was exposed to a strong mechanical load and confirms our aforementioned theory. Regarding technical applications, additional analysis methods besides classical microscopy could be necessary to analyze and minimize such material damage.

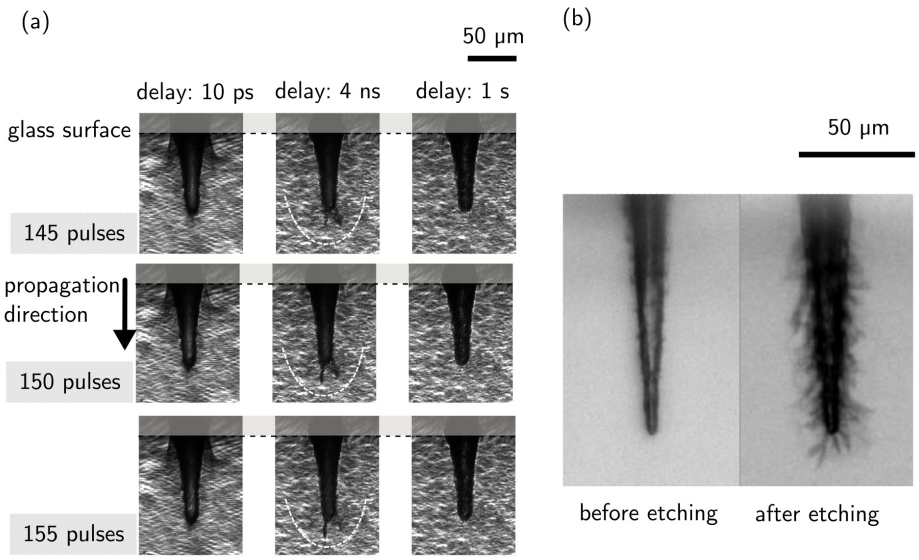

Fig. 3. Damage mechanisms on different timescales for ablation processing. The single pulse energy was chosen to 50 µJ with a pulse duration of 100 fs. The repetition rate was set to 1 Hz and the beam was focused by a lens with a focal length of 100 mm to the sample surface. Part (a) shows three selected frames from the movie in Visualization 1. In this movie, shadowgraph images at different delays are presented, where each frame represents one additional deposited pulse. Part (b) shows an ex-situ microscope image after 200 pulses before and after 10 minutes of etching in an 8 mol/l aqueous KOH solution at 85 °C.

Optics EXPRESS

4. Rear side ablation

To compare and investigate a different process, the following part deals with rear side ablation.

For this ablation technique, the absorption has to be localized on the rear side of the glass sample. Any absorption on the front, which causes ablation or other effects which result in a distortion of the beam propagation, should be avoided. Due to this reason the following experiment was conducted with a pump pulse duration of 5 ps and a pulse energy of 10 µJ at a repetition rate of 1 Hz. The beam was focused by a microscope objective with a focal length of 10 mm on the rear side of the 700 µm thick glass sample. The calculated spot size is 2 µm and the average fluence corresponds to 405 J/cm^2 . However, this value is never attained due to volume absorption in the converging beam. Hence, an increased free-electron density, which extends in propagation direction, is induced by the moving breakdown effect. For the applied pulse duration, the absorption starts at the focal position and extends along the isophote in direction of the incoming laser pulse within the first picoseconds [17].

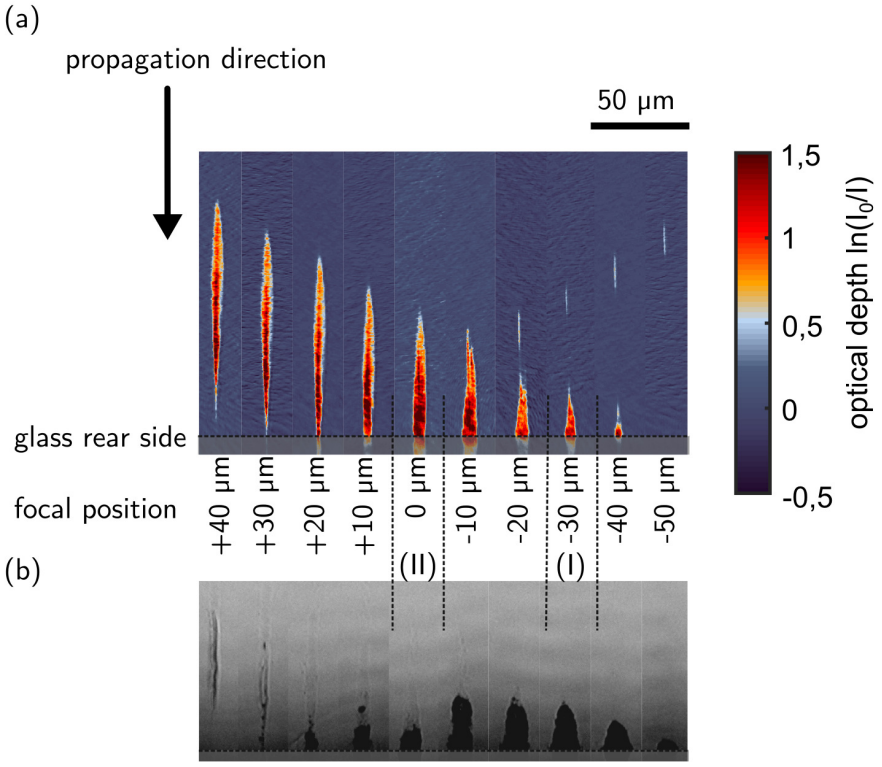

Fig. 4. Rear side ablation process at different focal positions. The pulse duration was set to 5 ps and a pulse energy of 10 µJ. The beam was focused by a microscope objective with a focal length of 10 mm at a repetition rate of 1 Hz. Part (a) shows the nonlinear absorption of the first deposited pulse with at a delay of 10 ps. Part (b) shows the corresponding modifications and ablation crater after 30 deposited pulses.

Figure. 4(a) shows the absorption zone at different focal positions on the glass rear side for the first deposited pulse in the pristine material. We applied a probe delay of 10 ps. From the left to the right, the microscope objective is moved in 10 µm steps from a focal position inside the

Optics EXPRESS

glass to a focal position below the glass rear side. The absorption zone shows the typical moving breakdown characteristic as aforementioned. When the focal position is set below the rear side of the workpiece, the reflectance of the incoming laser radiation at the glass air interface due to the refractive index mismatch causes a clearly visible excitation of the glass volume.

In Fig. 4(b) the corresponding, permanent modifications and the ablation craters after 30 deposited pulses at a repetition rate of 1 Hz are shown.

A maximum ablation depth can be observed for a focal position between 10 µm below the rear side of the workpiece and 30 µm. Whereas the focal position at the interface only produces a comparatively small ablation crater, surrounded by an extended modification. For a better understanding of this effect we present two cases in detail. The first (I), is the focal position with a maximum ablation depth and a minimum surrounding modification. Complemented by the second (II) focal position at the rear side of the sample with a large extended absorption zone but a reduced ablation depth.

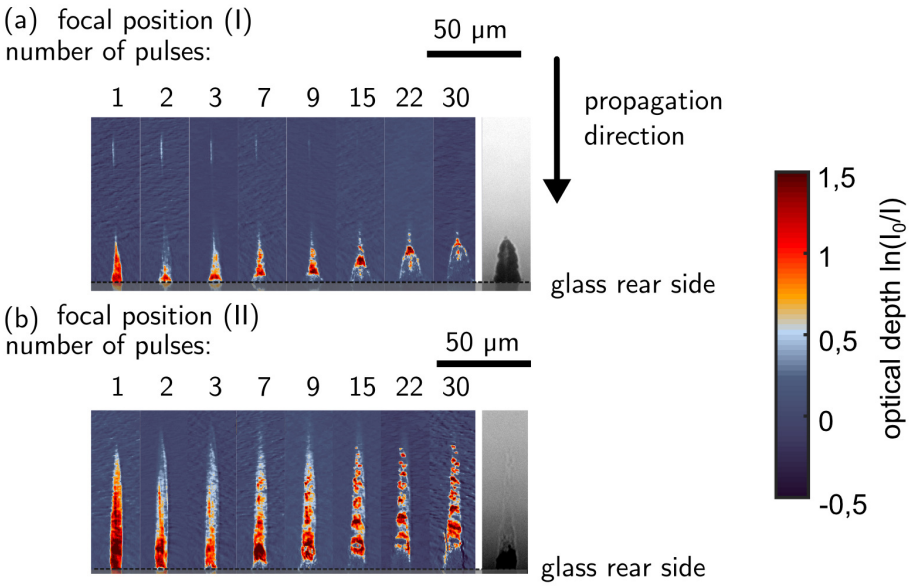

Fig. 5. Detailed crater and absorption evolution of focal position (I) and (II) from Fig. 4. The pulse duration was set to 5 ps. The beam was focused by a microscope objective with 10 mm focal length and a repetition rate of 1 Hz. The pulse energy was set to 10 µJ. Part (a) corresponds to the focal position (I) from Fig. 4. Part (b) shows the focal position (II) from Fig. 4. The delay was chosen to 10 ps for a maximized absorption zone. The final image on the right shows the permanent crater

In Fig. 5 the absorption zones for these two focal positions are shown for an increasing number of deposited pulses at a delay of 10 ps. Figure. 5(a) visualizes the corresponding experiments to case (I) of Fig. 4. The absorption zone starts with the rear part of the moving breakdown zone and then builds up a slight incubation effect over the following pulses. However, the absorption zone is strongly localized around the crater and the deposited energy results in material ablation. After 9 pulses the reflex at the rear side vanishes due to the crater formation. The ex-situ microscope image on the right shows no distinct modification around the crater.

In Fig. 5(b), the absorption zones for the focal position (II) of Fig. 4 are presented. The extended absorption zone shows a pronounced incubation effect for an increasing number of pulses. This modulation was also observed in our prior work for volume modifications [17]. In

Optics EXPRESS

our present experiments this modulation impedes the ablation process and leads to multiple permanent modifications above the crater which contribute to a shielding effect for subsequent pulses. Therefore, the free-electron density at the crater surface as well as the ablation depth is reduced compared to the focal position (I). In consequence, this extended free-electron density is not preferable for an efficient process.

The free-electron density should be generated exclusively close to the crater surface to avoid the generation of defects or any substantial modification in the volume of the workpiece, which surrounds the ablation crater. Additionally, a high NA enables the localized absorption on the rear side of the sample. For this purpose, the pulse energy should be drastically reduced compared to the latter experiments to minimize the moving breakdown and to generate the desired absorption zone at the focal position.

A similar optimized process regime can be accessed with an increased focal length and a reduced NA, respectively. As a consequence of the increased focal length, the excitation of the material shows a larger extent and can be investigated with an increased spatial resolution. However, this leads to a high sensitivity of the applied intensity and fluence, which has to be carefully adapted to avoid any absorption at the front surface.

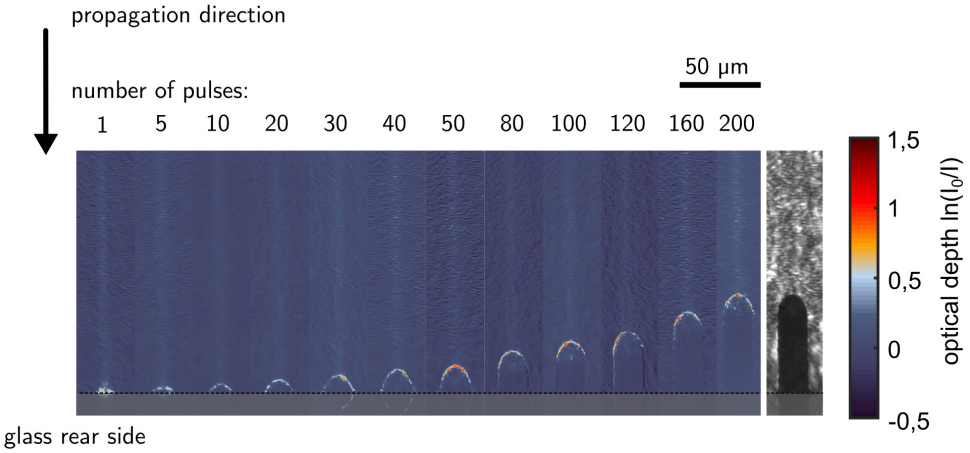

Fig. 6. Rear side ablation process with a pulse duration of 5 ps. The applied pulse energy was 20 µJ and the repetition rate was set to 1 Hz. The beam was focused by a lens with a focal length of 100 mm. The images show the nonlinear absorption zone at a delay of 10 ps as well as the permanent crater on the right.

Figure. 6 shows the resulting rear side ablation process with an increasing number of pulses. The pump pulse duration was set to 5 ps and the pulse energy to 20 µJ. The beam was focused by a lens with 100 mm focal length at a repetition rate of 1 Hz with a focal position slightly below the rear side. The resulting calculated average fluence is approximately 9 J/cm^2. The permanent crater after 200 pulses is shown on the right hand side. All images of the optical depth were recorded with a delay of 10 ps.

The absorption is mainly localized on the crater surface at the rear side of our sample, besides a negligible absorption zone perpendicular to the rear side, which results from the large Rayleigh length of approximately 283 µm. Thus a distinct modification inside the volume was not observed. In contrast to a front side ablation process, the refraction at the crater surface induces an increased intensity exclusively in the already ablated hole. Hence, further damage of the surrounding material can be avoided. In conclusion, the blind hole with a diameter of 20 µm and strongly reduced taper angles was drilled by a Gaussian beam focused in percussion mode, i.e. without any trepanning. We assume a stable process regime due to the fact, that the absorption zone

Optics EXPRESS

shows a marginal change while the crater geometry evolves over several pulses.

However, rear side ablation with the applied Rayleigh length impedes large scale, reproducible processing of thin samples or close to the front side. Therefore we will continue our in-situ investigations in future publications with a high NA setup and increased repetition rates to address robust processes with an increased throughput.

5. Conclusion

In this work, we conducted in-situ investigations of front and rear side ablation processes in alkali-aluminium-silica glass (nonstrengthened Corning Gorilla glass) with a thickness of 700 µm.

We examined the transverse absorption zones in the material during the formation of an ablation crater. These experiments showed an increased free-electron density which results in material damage due to refraction at the crater surface. Parameter variations reveal, that the absorption zone below the crater is more extended for pulse duration of 100 fs compared to a pulse duration of 5 ps at constant pulse energies. In this context rear side damage was detected for a pulse duration of 5 ps only. However, a pulse duration of 100 fs induced an increased free-electron density through the complete 700 µm thick material, but without sufficient energy to generate a central rear side ablation crater.

To investigate additional damage mechanisms we analyzed ablation process on an extended timescale. Our experiments reveal the formation of pressure waves and transient visible microcracks. These cracks were examined with nanosecond shadowgraphy and subsequent etching to analyze the material damage.

Compared to the front side ablation process, a high NA and high fluence regime was applied to study different focal positions at the rear side of the sample. These experiments reveal that a localized free-electron density leads to efficient ablation process compared to an extended free-electron density. In the latter case, incubation was identified to reduce the efficiency and quality of rear side ablation. The ideal process window was identified to a focal position 30 µm below the rear side to avoid modifications induced by the moving breakdown effect.

Finally we presented an ablation process in an optimized parameter regime to generate reduced taper angles with no damage of the surrounding material and a minimized absorption zone in the material by applying a pure percussion drilling process.

Funding

Federal Ministry of Education and Research (BMBF) (13N13309).